**Atmospheric
Chemistry
and Physics
Discussions**

Measurements of ambient HONO concentrations and vertical HONO flux above a northern Michigan forest canopy

N. Zhang[1], X. Zhou[1,2], S. Bertman[3], D. Tang[4], M. Alaghmand[5], P. B. Shepson[5], and M. A. Carroll[6]

[1]Department of Environmental Health Sciences, State University of New York, Albany, NY 12201, USA
[2]Wadsworth Center, New York State Department of Health, Albany, NY 12201, USA
[3]Department of Chemistry, Western Michigan University, Kalamazoo, MI 49008, USA
[4]Department of Psychology, Texas A&M University, College Station, TX 77843, USA
[5]Departments of Chemistry, Purdue University, West Lafayette, IN 47907, USA
[6]Department of Atmospheric, Oceanic and Space Science, University of Michigan, Ann Arbor, MI 48109, USA

Correspondence to: X. Zhou (zhoux@wadsworth.org)

Title Page

Abstract	Introduction
Conclusions	References
Tables	Figures

|◄ | ►|
◄ | ►

Back | Close

Full Screen / Esc

Printer-friendly Version

Interactive Discussion

Abstract

Systems have been developed and deployed at a North Michigan forested site to measure ambient HONO and vertical HONO flux. The modified HONO measurement technique is based on aqueous scrubbing of HONO using a coil sampler, followed by azo dye derivatization and detection using an optical fiber spectrometer with a 1-m long path flow cell. A Na_2CO_3-coated denuder is used to generate "zero HONO" air for background correction. The lower detection limit of the method, defined by 3 times of the standard deviation of the signal, is 1 pptv for 2-min averages, with an overall uncertainty of $\pm(1 + 0.05\,[\text{HONO}])$ pptv. The HONO flux measurement technique has been developed based on the relaxed eddy accumulation approach, deploying a 3-D sonic anemometer and two HONO measurement systems. The overall uncertainty is estimated to be within $\pm(8 \times 10^{-8} + 0.15\,F_{\text{HONO}})$ mol m^{-2} h^{-1}, with a 20-min averaged data point per 30 min. Ambient HONO and vertical HONO flux were measured simultaneously at the PROPHET site from 17 July to 7 August 2008. The forest canopy was found to be a net HONO source, with a mean upward flux of 0.37×10^{-6} moles m^{-2} h^{-1}. The HONO flux reached a maximum mean of $\sim 0.7 \times 10^{-6}$ moles m^{-2} h^{-1} around solar noon, contributing a major fraction ($\sim 60\%$) to the HONO source strength required to sustain the observed ambient concentration of ~ 70 pptv. There was no significant correlation between NO$_x$ and daytime HONO flux, suggesting that NO$_x$ was not an important precursor responsible for HONO daytime production on the forest canopy surface in the low-NO$_x$ rural environment. Evidence suggests that photolysis of HNO$_3$ deposited on the forest canopy surface is a major daytime HONO source.

1 Introduction

Nitrous acid (HONO) is a trace gas in the atmosphere, but it is an important component of NO$_y$. Photolysis of HONO produces hydroxyl radical (OH), the primary oxidant in the atmosphere responsible for the degradation of most of air pollutants and toxics. It

is estimated that HONO photolysis accounts for up to 80 % of OH production during early morning hours (Elshorbany et al., 2009; Ren et al., 2006; Vogel et al., 2003) and contributes to 20–60 % of the total OH production daily (Acker et al., 2006; Alicke et al., 2002, 2003; Kleffmann et al., 2005; Villena et al., 2011; Zhou et al., 2002a, 2007).

5 In addition, HONO is in an intermediate oxidation state and can be produced from nitrogen-containing precursors with higher oxidation states such as NO_2 and HNO_3, or lower oxidation states such as NO. HONO chemistry is essential in understanding the cycling of reactive nitrogen compounds in the troposphere.

Many studies indicated that most HONO observed in the atmospheric boundary layer
10 is produced by heterogeneous reactions on ground surfaces (including soil, buildings and vegetation) (Acker et al., 2004; Broske et al., 2003; Grassian, 2002; He et al., 2006; Kleffmann et al., 2003; Kleffmann and Wiesen, 2005; Ndour et al., 2008; Veitel et al., 2002; Zhang et al., 2009; Zhou et al., 2002a). To assess quantitatively the source strength on HONO on ground surface, measurement of exchange flux of HONO
15 between the ground and the atmosphere is essential. However, there are only a few HONO flux measurements reported in literature (Beine et al., 2005, 2006; Harrison and Kitto, 1994; Honrath et al., 2002; Ren et al., 2011; Stutz et al., 2002; Zhou et al., 2001, 2011); most of these HONO flux measurements were made based on an indirect gradient method, which is less accurate due to the large scatter of the concentration
20 measurements and the influence of chemical transformation during the turbulent transport process (Galmarini et al., 1997).

In the effort described here, a system was developed for direct measurement of HONO flux. It is based on a relaxed eddy accumulation technique (REA), which allows flux measurement with sensors that have much slower response time, such as gas
25 chromatography and mass spectrometry (Bowling et al., 1998). This REA technique has been successfully used to measure a number of chemical species, such as CO_2, H_2O, N_2O and biogenic VOCs. Comparison studies have shown excellent agreement between fluxes of reactive compounds determined by Eddy covariance (EC) and REA techniques (Bowling et al., 1998; Pattey et al., 1993; Westberg et al., 2001). Here we

Full Screen / Esc

Printer-friendly Version

Interactive Discussion

report measurements of HONO flux, along with HONO ambient concentrations over a forest canopy, using REA coupled with two modified HONO measurement systems based on coil sampling, azo dye derivatization and long-path flow cell photometric detection (Huang et al., 2002; He et al., 2006). The results quantitatively reveal the role of ground surfaces on HONO heterogeneous formation.

2 Experimental

2.1 Site description

HONO concentration and flux were simultaneously measured on a 31-m scaffolding tower at the PROPHET site at the University of Michigan Biological Station (45°30′ N, 84°42′ W, elevation 238 m) from 17 July to 7 August 2008. The PROPHET site is located in an undisturbed and well-characterized, mixed deciduous/coniferous forest with the major tree species of aspen, maple, red oak, pine and beech. Average canopy height is ~21 m. Air masses reaching this site are dominated by westerly flow: southwesterly flow is generally polluted air from metropolitan and industrial areas (e.g. Chicago and Milwaukee) and northwesterly flow is relatively clean air from Canada (Cooper et al., 2001). A complete description of the site has been given in (Carroll et al., 2001).

2.2 HONO concentration measurement

Three HONO measurement systems (Fig. 1), a modification based on the method of Huang et al. (2002) and He et al. (2006), were used in this study: one for ambient concentration measurement and two for flux measurement (described below). Briefly, ambient HONO was scrubbed by de-ionized (DI) water (resistance >18.2 MΩ cm) using a coil sampler; the scrubbed nitrite was derivatized with 2 mM sulfanilamide (SA) and 0.2 mM n-(1-naphthyl)-ethylenediamine (NED) in a 1-ml thermostatic derivatization coil at 50 °C. The azo dye derivative was quantified by light absorbance at 540 nm

using a miniature fiber optic spectrometer (USB2000, Ocean Optics) with a 1-m liquid-waveguide capillary flow cell (WPI). The system was operating on a 30-min cycle controlled by a 3-way solenoid valve: sampling ambient air for 20 min (measurement mode) and then "zero-HONO" air for 10 min to obtain a baseline (zero mode). The zero air was generated by pulling ambient air through a $NaCO_3$ coated annular denuder. Gaseous acidic species, including HONO, are quantitatively removed by the denuder, but aerosols and most other gases, including potential interferences such as NO_x, are allowed to pass through (USEPA, 1999). The absorbance signal collection frequency was 0.3 Hz.

2.3 REA flux system

The HONO flux system was developed based on the relaxed eddy accumulation (REA) technique which involves conditional sampling of air into updraft and downdraft components at a constant flow rate (Bowling et al., 1998). The duration of sampling for each component is only related to the frequency at which the wind eddy changes in vertical direction. Air samples collected in each component were accumulated over a collection period before determination of concentrations. The Flux (F) is calculated using the following relationship (Businger and Oncley, 1990):

$$F = \beta \sigma_w (\bar{C}_{up} - \bar{C}_{dn}) \tag{1}$$

where β is an empirically determined coefficient with a value of $\sim$0.6 over a smooth surface (Businger and Oncley, 1990; Westberg et al., 2001), σ_w is the standard deviation of vertical wind sector over the collection period, and $\bar{C}_{up}$ and $\bar{C}_{dn}$ are the average concentrations of HONO in the updraft and downdraft components, respectively.

The HONO flux measurement system is illustrated in Fig. 2, consisting of a three-dimensional sonic anemometer and two HONO measurement systems. A CSAT3 3-D sonic anemometer (Campbell Scientific) was mounted at $\sim$11 m above the canopy level on an arm extending $\sim$1.5 m away from the west side of the tower facing the prevailing wind and used to acquire wind speed at 10 Hz. During flux measurement,

the value of σ_w was determined by the vertical wind from the previous 30-min period. A dynamic threshold (deadband) $w_T = \sigma_w/2$ was used to increase the concentration difference between the reservoirs (Bowling et al., 1998; Pattey et al., 1993). The vertical component of the instantaneous wind velocity, w, was compared to a threshold w_T.

5 Based on this comparison, a laptop computer was used to control the switching of two 3-way valves for conditional sampling (Table 1): for $w > w_T$, ambient air was collected into an updraft component and zero air flows through a downdraft component; for $w < -w_T$, ambient air was sampled into a downdraft component and zero air flows through an updraft component; for $-w_T < w < w_T$, zero air flew into both components.

10 A deadband can be used to improve the sensitivity of the measurement and prolong the life of the REA valves. However, a deadband will result in some uncertainty in the concentration difference measurement by decreasing the effective sampling time (Oncley et al., 1993). A reduction of the coefficient β was also reported to be associated with the use of a deadband (Pattey et al., 1993). In our experiment, data collected

15 during very calm periods (i.e., when $|w| \leq w_T$ for more than 95 % of the sampling period) were excluded in flux calculations.

Two HONO measurement systems described above were used to measure HONO concentrations in the up and down air drafts. The systems were operated over the same 30-min cycle as the ambient measurement system. During the 20-min measurement

20 mode, both up and down systems were doing conditioned sampling (Table 1). Sample flow rate in each of the three channels (Up + Down + Ambient) was maintained at a constant rate of 2 l min^{-1}. Ambient air was pulled into scrubbing samplers through a 2.2-m PFA tube (3.2-mm ID) inlet extended near the anemometer probe at a total flow rate of 6 l min^{-1}. A 200 ms delay before valves responded to the vertical wind signal

25 was set to compensate for time lags from the inlet to REA valves. A LabVIEW program was developed for the communication with the sonic anemometer and REA valves.

2.4 Calibration

Calibration was performed by introducing aqueous $NaNO_2$ standard solutions in place of scrubbing solution into the HONO measurement system in the zero mode. The signal height was plotted against the nitrite concentration to yield a calibration curve for the ambient concentration channel. For HONO flux measurement, the signal area was integrated above the baseline and was plotted against the amount of nitrite, calculated from the $NaNO_2$ standard concentration, delivery flow rate and time. Three full range, multipoint calibrations were conducted at the beginning, middle, and end of the campaign. A single point calibration was made for every batch of reagent solutions, which usually lasted for 2 days. Correlation coefficients r^2 were ≥ 0.999 for both sets of calibration curves.

2.5 HONO photolysis rate constant

The total solar ultraviolet intensity (295–385 nm) was measured using an Eppley TUVR radiometer ($UV^{measured}$) with a detection limit of $0.3\,W\,m^{-2}$ and overall uncertainty of 10 % (Carroll et al., 2001). The radiative transfer model (http://cprm.acd.ucar.edu/Models/TUV/Interactive_TUV/) was used to calculate HONO photolysis rate constant (J_{HONO}^{model}) and total UV intensity between 295 nm and 385 nm (UV^{model}) for clear sky conditions, taking into account the climatological O_3 column and aerosol optical depth, time of day and month, and location of the sampling site. Correction was made for variable cloud cover using the following equation (Kleinman et al., 1995):

$$J_{HONO} = J_{HONO}^{model} \times (UV^{measured} / UV^{model})/(UV^{measured*}/UV^{model*}) \qquad (2)$$

where the $UV^{measured*}$ and UV^{model*} are the modeled and measured UV intensities at solar noon under clear sky.

2.6 NO$_x$ measurements

NO$_x$: NO and NO$_2$ were measured with a custom-built analyzer using the chemiluminescence technique constructed as described by Ridley and Grahek (1990) and Alaghmand et al. (2011). The chemiluminescence photons were detected using a Burle Industries 8852 photomultiplier tube, cooled with dry ice, and a Hamamatsu photon counting system. The instrument incorporates a blue light LED NO$_2$ photolytic converter. The average NO$_2$ conversion efficiency for a flow rate of 1.2 slpm was determined to be 28.6 ± 0.9 %. For 5-min averaged data, the detection limit was 7 pptv for both NO and NO$_2$.

2.7 Meteorological parameters

Temperature, dew point, precipitation, relative humidity and weather conditions were acquired through the website (http://www.wunderground.com). Back trajectories at both 50 m and 500 m above the ground levels were calculated using HYSPLIT (HYbrid Single-Particle Lagrangian Integrated Trajectory) Model (Draxler and Rolph, 2003) to identify the air source region.

3 Results and discussion

3.1 Ambient HONO system performance

Two major modifications were made to the original method of Huang et al. (2002), including: (1) HPLC/UV-vis detection technique was replaced by a long-path photometric technique using a miniature fiber optic spectrometer with a 1-m flow cell, and (2) a 3-way solenoid valve was used to alternately introduce ambient air or "zero-HONO" air to a coil sampler. The sensitivity of the long-path photometric technique is greatly enhanced compared to the conventional spectrophotometric method, by two orders of magnitude (He et al., 2006). It eliminates the use of organic solvents as a mobile phase

in the HPLC method, which is a significant advantage since organic solvent usage in the field may interfere with measurements of organic species. The light absorbance signal was collected at a rate of 0.3 Hz, with an alternated sampling cycle of ambient air and "zero-HONO" air. While the Na_2CO_3 coated denuder removed HONO and acidic gases from the ambient air, it allowed most of the potential interfering species such as NO, NO_2, PAN, nitrate and aerosol, to pass (USEPA, 1999). Therefore, interference from these species was mostly eliminated by subtracting the "zero-HONO" signals from the ambient air signals.

Figure 3 shows an excerpt of 10-min raw data recorded in the morning of 25 July 2008. The 90 % response time, based on the signal transition from "zero-HONO" air to ambient air, was about 110 s. The response time may be shortened by increasing the rates of scrubbing and reagent flows and by reducing the length of tubing in the liquid flow plumbing. The ambient concentrations were derived from the difference between the ambient signals and the "zero-HONO" air. The "zero-HONO" baseline drifted only slowly throughout the day in response to factors including concentrations of interfering species (e.g. NO_x), temperature and reagent age. The baseline drift was within 20 pptv day^{-1}, with a minimum a few hours after midnight and a maximum in the mid afternoon. After removing the transitional data points, 17–18 min of ambient HONO concentration data were collected in each 30-min cycle (Fig. 4, lower panels). The raw data were reduced into 2-min averages.

The lower detection limit of the method is estimated to be ~1 pptv, based on 3 times the standard deviation of the zero air signal. The linear dynamic range is 1–5000 pptv; above 5000 pptv, the signal becomes non-linear. The upper limit of linear dynamic range can be improved by increasing the rates of scrubbing and reagent flows and by reducing the air sampling flow rate. These measures, however, will increase the lower detection limits. The measurement precision, based on side-by-side measurements using multiple HONO systems, is estimated to be better than 2 % in the concentration range of 50 pptv to 5 ppbv. An overall uncertainty of $\pm(1 + 0.05 \text{ [HONO]})$ pptv

is estimated, accounting for uncertainties in signal acquisition and processing, air and liquid flow rates, and standard preparation.

3.2 HONO flux system performance

As most surfaces are not perfectly flat, the vertical wind fluctuations are often affected by the mean horizontal wind (Chahuneau et al., 1989). During the 2 weeks prior to the measurement of HONO flux at the site, 3-D wind data were collected by the anemometer. The collected wind data were used for coordinate transformation, which aligned wind data collected during flux measurement with the mean wind streamlines, thus when $w = 0$, the average flux of dry air perpendicular to the surfaces of interest is zero. An example of raw data for vertical wind velocity by the anemometer and HONO signals recorded by the spectrometers are shown in the upper panels in Fig. 4. It is apparent that the vertical wind fluctuated around zero (red trace), with the length of individual updraft or downdraft capable of triggering the valves (i.e. $|w| > w_T$) in the range of 0.1–20 s, resulting in ambient air sampling in the updraft channel ($w > w_T$) or in the downdraft channel ($w < -w_T$). The signals of the two HONO flux traces for the updraft (red trace) and the downdraft (green trace) (Fig. 4, upper panels) was lower than that for ambient concentration channel (blue) since the flux valves opened to the ambient air only fractions of the time during the 20-min sampling period when $|w| > w_T$.

To quantify HONO collected in each channel during each sampling period, the area of the signal above the "zero-HONO" air baseline was integrated and converted into moles of HONO sampled based on the calibration curve. The integrated HONO concentration was derived from the moles of HONO divided by the ambient air volume sampled when the valve was triggered. The middle panel in Fig. 4 shows the integrated concentrations in the updraft and downdraft channels along with the standard deviation of vertical wind (σ_w) during the sampling cycle. The 20-min averaged HONO flux was then derived from the σ_w, $\bar{C}_{up}$ and $\bar{C}_{dn}$ information in the middle panel using Eq. (1) (lower panel, Fig. 4).

Full Screen / Esc

Printer-friendly Version

Interactive Discussion

To ensure the data quality, data collected in very calm periods were not used for flux calculation, i.e., when $|w| \leq w_T$ for more than 95 % of the sampling period. The flux values were usually low during very calm periods, due to the small σ_w. The overall precision is estimated to be within $\pm(8 \times 10^{-8} + 0.15\,F_{HONO})\,\mathrm{mol\,m^{-2}\,h^{-1}}$, estimated from uncertainties associated with HONO measurements in both up and down channels, the volume of ambient air collected during the periods when the valve was triggered ($w > w_T$ for the updraft channel and $w < -w_T$ for the downdraft channel), and the σ_w derived from vertical measurement.

An REA-HONO system has been recently reported (Ren et al., 2011), based on the same principles. However, there were several differences in the HONO measurement setups, which might affect the system performance. In our system, the "zero-HONO" air was generated by pulling ambient air through a $NaCO_3$ coated annular denuder and was used to establish a measurement baseline in a 30-min cycle. Since most of the potential interfering species such as NO_x, PAN, nitrate and aerosol pass the denuder (USEPA, 1999), interference from these species was mostly eliminated by subtracting the "zero-HONO" baseline signal from the ambient air signals. Frequent baseline correction under this setup also minimized the HONO measurement uncertainty caused by baseline drift and thus improved measurement accuracy. Furthermore, two dedicated HONO measurement systems were used in the HONO flux measurement, simultaneously measuring HONO concentrations in the updraft and the downdraft air masses within a sampling cycle, with better time resolution.

3.3 Measurement results

3.3.1 Data statistics

A highlight of the HONO flux measurement results has been published elsewhere (Zhou et al., 2011). A complete data set with discussions of cases is presented here. Figure 5 shows HONO fluxes and ambient HONO concentrations during the measurement campaign. Overall, upward HONO fluxes were observed most of the time over the

measuring period, with occasional downward fluxes during rain, fog and dew events. An upward maximum of 4.7×10^{-6} moles m^{-2} h^{-1} was observed during the day after a high NO$_x$ and NO$_y$ event, a downward maximum of about 2×10^{-6} moles m^{-2} h^{-1} during a rain event, with a mean of 0.37×10^{-6} moles m^{-2} h^{-1}. Ambient HONO con-
centrations ranged from 10 pptv during rain events to 189 pptv during a pollution event at night, with a mean of 49 pptv. On average, both the HONO flux and ambient concentration exhibited noontime maxima, at $\sim 0.7 \times 10^{-6}$ moles m^{-2} h^{-1} and ~ 70 pptv, respectively. The minimum of the average HONO flux was about $\sim 0.1 \times 10^{-6}$ moles m^{-2} in the early morning before sunrise, and minimum average HONO concentration was
~ 20 pptv around the time of sunset (Zhou et al., 2011). On average, the photolysis of HONO contributed about 340 pptv h^{-1} of OH production, similar to those reported for this and other rural sites, between 250–560 pptv h^{-1} (Acker et al., 2006; Zhang et al., 2009; Zhou et al., 2007).

The only other REA HONO flux measurement in the low-NO$_x$ rural environment was made at the Blodgett Forest site in California (Ren et al., 2011). The reported daytime mean HONO flux, $(-0.014 \pm 0.086) \times 10^{-6}$ moles m^{-2} h^{-1}, was much lower than that observed at the PROPHET site. Such a large difference in HONO fluxes at the two rural and forested sites may largely be attributed to the difference in acidity/pH of canopy surfaces and soils. The overall pH in precipitation and thus of the soil and canopy surfaces in the western US including California, is significantly higher than in the midwestern and northeast US, by 2 pH units (National Atmospheric Deposition Program (NADP), http://nadp.sws.uiuc.edu). Since HONO is a weak acid, with a pKa of 3.5, the HONO-nitrite equilibrium would shift to nitrite with higher pH. At elevated pH, canopy and ground surfaces would behave more like a sink than a source for HONO at the Blodgett Forest site (Ren et al., 2010, 2011). In the Mid West and Northeast, on the other hand, HONO can be readily released into the atmosphere from acidic canopy and ground surfaces once produced (He et al., 2006), and becomes a major HONO source for the overlying atmosphere (He et al., 2006; Zhou et al., 2002a, 2007, 2011).

3.3.2 Forest canopy as a HONO source or a sink

In forested areas, forest canopy surfaces account for the majority of the surface area in the atmospheric boundary layer, thus serve as sites for the heterogeneous reaction leading to HONO formation under favorable conditions. Indeed, the canopy was a net source for HONO at UMBS most of the time indicated by the observed upward HONO flux (Fig. 5). However, the canopy can also be a net HONO sink, as indicated by occasional downward fluxes during rain events (e.g. 17, 20, 29 July), and fog and dew events (e.g. 19, 27 July) (Fig. 5). The wet canopy seemed to enhance the dry deposition of HONO and/or prevent HONO from being released once produced by heterogeneous reactions, in agreement with previous observations (e.g. Zhou et al., 2002a; He et al., 2006).

Figure 6 shows the effect of vertical wind variability on HONO transport. On average, HONO concentrations were about 8 % higher in the updraft air than in the downdraft air, with increasing variability at lower s_w. Lower s_w tended to occur during the night (Fig. 5) when the air was more stable due to surface cooling. During the nights that were free of rain or dew, the canopy surface would act as a HONO source, and steeper negative vertical HONO gradients would develop under stagnant conditions, resulting in positive spreads in the HONO concentration difference (He et al., 2006; Zhou et al., 2011). However, dew and mist events occurred in some calm and clear nights, and dry deposition of HONO was enhanced by the wet canopy, resulting in the negative spread of HONO concentration difference (Fig. 6) (He et al., 2006; Zhou et al., 2011). There is a general trend of higher HONO flux with higher s_w, as expected from Eq. (1). However, the maximum fluxes, both upward and downward, occurred at the mid range s_w values. The highest upward fluxes occurred around solar noon during the days after passing urban plumes deposited HONO precursors on the canopy, for example, on 18 July and 5 August (see more discussion in Case Study below). The highest downward fluxes occurred during a thunder storm in the afternoon of 20 July (Fig. 5).

Substantial levels of HONO existed during the day, despite the effective photolytic loss, reaching an average maximum of about 70 pptv around solar noon. To sustain the observed concentration, a strong HONO source, about 350 pptv h^{-1} on average around noontime, was needed. Zhou et al. (2011) estimated the effect of canopy surface on the observed HONO mixing ratios, based on a 1-D transport of HONO from the canopy, assuming that midday HONO flux of $\sim$7 $\times$ 10^{-7} moles m^{-2} h^{-1}, a HONO photolysis rate constant of $\sim$5 h^{-1}, and a eddy diffusivity coefficient (Kz) of $\sim$3.6 $\times$ 10^4 m^2 h^{-1} (or $\sim$1 $\times$ 10^5 cm^2 s^{-1}). Indeed, calculations indicated that this source of HONO accounted for the majority of the observed HONO, $\sim$57 % on average, at the observation height of 32 m above ground, and the remaining 43 % was from volume HONO production mechanisms, such as gaseous NO-OH reactions, and more likely, heterogeneous reactions involving NO$_x$ and HNO$_3$ on aerosol surface (Zhou et al., 2011).

3.3.3 HONO precursors

It is generally believed that atmospheric HONO is produced mostly by heterogeneous reactions involving HONO precursors such as NO$_x$ (George et al., 2005; Lammel and Cape, 1996; Stemmler et al., 2006, 2007) and HNO$_3$ (Zhou et al., 2002a, 2002b, 2003, 2007, 2011). In low-NO$_x$ environments, photolysis of HNO$_3$ deposited on ground/canopy surface has been proposed to be the major daytime HONO source (Zhou et al., 2002a, 2003, 2007). To test this hypothesis, 16 sets of leaf samples (6 leaves per set) were collected at the top of the forest canopy for surface nitrate measurement (Zhou et al., 2011). The daytime HONO flux was found to be strongly correlated (r^2 = 0.69) with the surface nitrate photolysis potential, defined as the product of surface nitrate loading and the surface nitrate photolysis rate constant calculated from Eppley UV intensity. Therefore, it was concluded that photolysis of HNO$_3$ deposited on the canopy surface was the major mechanism responsible for the observed daytime HONO flux from the canopy into the atmosphere (Zhou et al., 2011).

The concentrations of NO$_x$ and HONO, and the HONO flux were measured simultaneously over two weeks (Figs. 7, 8), allowing us to examine the role of NO$_x$ as a

HONO precursor at this site. During the day, NO_x and the HONO flux were found not to be correlated at any significant level ($r^2 = 0.01$), suggesting NO_x was not a significant daytime HONO precursor responsible for the upward flux from the forest canopy. The correlation between NO_x and the daytime HONO concentration is slightly improved but still weak ($r^2 = 0.10$), reflecting some degree of contribution from the volume HONO production under high-NO_x conditions during southerly flow. During the nights that were free of rain or dew, the contribution of the dark heterogeneous NO_x reaction to the observed HONO flux increased, as indicated by the improved correlation between HONO flux and NO_x ($r^2 = 0.37$, Fig. 7). The even stronger correlation between concentrations of HONO and NO_x ($r^2 = 0.56$, Fig. 7) accounts for both the HONO produced at the forest canopy and the HONO transported in the air mass, and suggests that NO_x was the major HONO precursor when photolysis of HNO_3 on surface was absent.

3.3.4 A case study

The behavior of HONO during the initial two days of this campaign is examined in more detail to illustrate the processes discussed above as a case study (Fig. 8). During the morning of 17 July before sunrise, the concentrations of HONO and NO_x varied in sync when air masses switched from clean northwesterly flow to more polluted southwesterly flow (Cooper et al., 2001). Both ambient HONO and NO_x concentrations were rising rapidly, from 40 pptv to 160 pptv and from 700 pptv to 2600 pptv, respectively. The strong correlation between the concentrations of HONO and NO_x ($r^2 = 0.89$, $N = 7$, hourly averages) and the slightly negative HONO flux during the early morning period suggests that most of the observed ambient HONO during the period was produced within the air mass on the way to the measurement site, probably by heterogeneous NO_x reactions on aerosol surfaces.

After sunrise, the HONO flux was mostly positive, reaching $\sim 1.7 \times 10^{-7}$ moles m^{-2} h^{-1} around 11:00 EDT, with the exception of a slightly negative flux ($\sim -0.1 \times 10^{-7}$ moles m^{-2} h^{-1}) at 11:30 EDT when NO_x reached a peak

of 4500 pptv. Several similar brief negative HONO fluxes occurred throughout the campaign, mostly coinciding with rapid increase in NO_x and with relatively high ambient HONO concentrations. This phenomenon may be caused by the concentration diffusion from elevated levels of HONO in the air above down to the relatively clean air within the forest canopy during the early phase of pollution episodes.

In the afternoon, the HONO flux remained significantly positive, between 0.1 and 1.1×10^{-6} moles m^{-2} h^{-1} despite the significant decrease in NO_x to around 1000 pptv. Furthermore, both the HONO flux and ambient HONO concentrations seemed to modulate with the fluctuation of HONO photolysis rate constant, suggesting significant contribution of photochemical production of HONO at the forest canopy to the overlying atmosphere.

Light rain and drizzle started around 08:00 p.m. (EDT) and continued intermittently throughout the night, as indicated by the thick line on the x-axis of the upper panel in Fig. 8. When surfaces were wet, the forest canopy became a sink rather than a source for HONO (He et al., 2006; Zhou et al., 2011). As a result, the net HONO flux was negative, and ambient HONO concentrations remained low, mostly within 20–30 pptv. However, there was significant fluctuation in HONO flux before and around midnight, probably due to high wind variability during this period. The following period (04:00–07:00 EDT) was very calm with the vertical wind speed w lower than the threshold w_t value of 0.1 m s^{-1} (Fig. 5), resulting in a data gap in HONO flux.

It was intermittent clouds in the morning of 18 July; both HONO flux and ambient HONO concentrations remained low. The sky became clear shortly after noontime; both the HONO flux and ambient HONO concentration started to increase, reaching a HONO flux maximum of 4.6×10^{-6} moles m^{-2} h^{-1} and a maximum daytime HONO concentration of 165 pptv in the early to mid afternoon. It is especially worthy to point out that the air arriving at the site during this period of time changed from southwesterly (polluted) to northwesterly (clean), and that NO_x levels dropped from ~1500 pptv to ~400 pptv. This anti-correlation between NO_x and HONO flux suggests that ambient NO_x was not a significant precursor for the HONO produced at the canopy surface.

During the southwesterly flow period during the previous day and night, HNO_3 as well as organics might have deposited from the "dirtier" southwesterly air mass and accumulated on the leaf surfaces at the top of forest canopy. When exposed to solar UV radiation, the photolysis of the deposited HNO_3 (Zhou et al., 2003, 2011), enhanced by the presence of organics (Zhang et al., unpublished data), was probably the dominant HONO production mechanism responsible for the higher upward flux and the high ambient HONO concentration.

The HONO flux as well as the ambient HONO concentration decreased in the late afternoon and evening as the solar radiation and the photolytic HONO source decreased. There were, however, some spikes in HONO flux and HONO concentration before midnight, probably associated with a change in air masses. Indeed, the back trajectory calculation indicates that air flow changed from northwesterly to southwesterly and then back to northwesterly during the ∼4 h before midnight.

4 Summary and conclusions

1. A HONO measurement method (Huang et al., 2002; He et al., 2006) has been modified and improved, based on aqueous scrubbing of HONO using a coil sampler, followed by azo dye derivatization and detection using an optical fiber spectrometer with a 1-m long path flow cell. A Na_2CO_3-coated denuder is used to generate "zero HONO" air for background correction. The lower detection limit of the method, as defined by 3 times the standard deviation of the signal, is 1 pptv for 2-min averages, with an overall uncertainty of $\pm(1 + 0.05 \, [HONO])$ pptv.

2. A HONO flux measurement technique has been developed based on the relaxed eddy accumulation approach. One 3-D sonic anemometer and two HONO measurement systems were deployed in this field campaign. The overall precision is estimated to be within $\pm(8 \times 10^{-8} + 0.15 \, F_{HONO}) \, \text{mol m}^{-2} \, \text{h}^{-1}$, with 20-min averaged data point per 30 min.

3. The techniques for ambient HONO and HONO flux measurements have been successfully deployed at the PROPHET site during the summer of 2008. The mean HONO concentration was 49 pptv and mean HONO flux was 0.37×10^{-6} moles m^{-2} h^{-1}. Both HONO and HONO flux showed significant diurnal variations, with maximum means of $\sim$70 pptv and $\sim$0.7 $\times 10^{-6}$ moles m^{-2} h^{-1}, respectively, in the early afternoon, and a HONO minimum mean of $\sim$20 pptv around the time of sunset, and a minimum HONO flux mean of $\sim$0.1 $\times 10^{-6}$ moles m^{-2} in the early morning before sunrise.

4. In the low-NO$_x$ atmospheric boundary layer over a forest, photolysis of HNO$_3$ deposited on the top of canopy was the major HONO source during the day, while the heterogeneous reactions of NO$_2$ on canopy and aerosol surfaces was dominant at night.

References

Acker, K., Spindler, G., and Bruggemann, E.: Nitrous and nitric acid measurements during the INTERCOMP2000 campaign in Melpitz, Atmos. Environ., 38, 6497–6505, 2004.

Acker, K., Moller, D., Wieprecht, W., Meixner, F. X., Bohn, B., Gilge, S., Plass-Dulmer, C., and Berresheim, H.: Strong daytime production of OH from HNO$_2$ at a rural mountain site, Geophys. Res. Lett., 33, L02809, doi:10.1029/2005GL024643, 2006.

Alaghmand, M., Shepson, P. B., Starn, T. K., Jobson, B. T., Wallace, H. W., Carroll, M. A., Bertman, S. B., Lamb, B., Edburg, S. L., Zhou, X., Apel, E., Riemer, D., Stevens, P., and Keutsch, F.: The Morning NO$_x$ maximum in the forest atmosphere boundary layer, Atmos. Chem. Phys. Discuss., 11, 29251–29282, doi:10.5194/acpd-11-29251-2011, 2011.

Alicke, B., Platt, U., and Stutz, J.: Impact of nitrous acid photolysis on the total hydroxyl radical budget during the Limitation of Oxidant Production/Pianura Padana Produzione di Ozono study in Milan, J. Geophys. Res., 107, 8196, doi:10.1029/2000JD000075, 2002.

Alicke, B., Geyer, A., Hofzumahaus, A., Holland, F., Konrad, S., Patz, H. W., Schafer, J., Stutz, J., Volz-Thomas, A., and Platt, U.: OH formation by HONO photolysis during the BERLIOZ experiment, J. Geophys. Res., 108, 8247, doi:10.1029/2001JD000579, 2003.

Beine, H. J., Amoroso, A., Esposito, G., Sparapani, R., Ianniello, A., Georgiadis, T., Nardino, M., Bonasoni, P., Cristofanelli, P., and Domine, F.: Deposition of atmospheric nitrous acid on alkaline snow surfaces, Geophys. Res. Lett., 32, L10808, doi:10.1029/2005GL022589, 2005.

Beine, H. J., Amoroso, A., Dominé, F., King, M. D., Nardino, M., Ianniello, A., and France, J. L.: Surprisingly small HONO emissions from snow surfaces at Browning Pass, Antarctica, Atmos. Chem. Phys., 6, 2569–2580, doi:10.5194/acp-6-2569-2006, 2006.

Bowling, D. R., Turnipseed, A. A., Delany, A. C., Baldocchi, D. D., Greenberg, J. P., and Monson, R. K.: The use of relaxed eddy accumulation to measure biosphere-atmosphere exchange of isoprene and of her biological trace gases, Oecologia, 116, 306–315, 1998.

Bröske, R., Kleffmann, J., and Wiesen, P.: Heterogeneous conversion of NO_2 on secondary organic aerosol surfaces: A possible source of nitrous acid (HONO) in the atmosphere?, Atmos. Chem. Phys., 3, 469–474, doi:10.5194/acp-3-469-2003, 2003.

Businger, J. A. and Oncley, S. P.: Flux Measurement with Conditional Sampling, J. Atmos. Ocean. Tech., 7, 349–352, 1990.

Carroll, M. A., Bertman, S. B., and Shepson, P. B.: Overview of the Program for Research on Oxidants: PHotochemistry, Emissions, and Transport (PROPHET) summer 1998 measurements intensive, J. Geophys. Res., 106, 21275–24288, doi:10.1029/2001JD900189, 2001.

Chahuneau, F., Desjardins, R. L., Brach, E., and Verdon, R.: A Micrometeorological Facility for Eddy Flux Measurement of CO_2 and H_2O, J. Atmos. Ocean. Tech., 6, 193–200, 1989.

Cooper, O. R., Moody, J. L., Thornberry, T. D., Town, M. S., and Carroll, M. A.: PROPHET 1998 meteorological overview and air-mass classification, J. Geophys. Res., 106, 24289–24299, doi:10.1029/2000JD900409, 2001.

Draxler, R. R. and G. D. Rolph: HYSPLIT (HYbrid Single-Particle Lagrangian Integrated Trajectory) Model access via NOAA ARL READY Website (http://www.arl.noaa.gov/ready/hysplit4.html), NOAA Air Resources Laboratory, Silver Spring, MD, 2003.

Elshorbany, Y. F., Kleffmann, J., Kurtenbach, R., Rubio, M., Lissi, E., Villena, G., Gramsch, E., Rickard, A. R., Pilling, M. J., and Wiesen, P.: Summertime photochemical ozone formation in Santiago, Chile, Atmos. Environ., 43, 6398–6407, 2009.

Galmarini, S., DeArellano, J. V. G., and Duyzer, J.: Fluxes of chemically reactive species inferred from mean concentration measurements, Atmos. Environ., 31, 2371–2374, 1997.

George, C., Strekowski, R. S., Kleffmann, J., Stemmler, K., and Ammann, M.: Photoenhanced uptake of gaseous NO_2 on solid organic compounds: a photochemical source of HONO? Faraday Discuss., 130, 195–210, 2005.

Grassian, V. H.: Chemical reactions of nitrogen oxides on the surface of oxide, carbonate, soot, and mineral dust particles: Implications for the chemical balance of the troposphere, J. Phys. Chem. A, 106, 860–877, 2002.

Harrison, R. M. and Kitto, A-M. N.: Evidence for a surface source of atmospheric nitrous acid, Atmos. Environ., 28, 1089–1094, 1994.

He, Y., Zhou, X., Hou, J., Gao, H., and Bertman, S. B.: Importance of dew in controlling the air-surface exchange of HONO in rural forested environments, Geophys. Res. Lett., 33, L02813, doi:10.1029/2005GL024348, 2006.

Honrath, R. E., Lu, Y., Peterson, M. C., Dibb, J. E., Arsenault, M. A., Cullen, N. J., and Steffen, K.: Vertical fluxes of NO_x, HONO, and HNO_3 above the snowpack at Summit, Greenland, Atmos. Environ., 36, 2629–2640, 2002.

Huang, G., Zhou, X., Deng, G., Qiao, H., and Civerolo, K.: Measurements of atmospheric nitrous acid and nitric acid, Atmos. Environ., 36, 2225–2235, 2002.

Kleinman, L., Lee, Y.-N., Springston, S. R., Lee, J. H., Nunnermacker, L., Weinsten-Lloyd, J., Zhou, X., and Newman L.: Peroxy radical concentration and ozone formation rate at a rural site in southeastern United States, J. Geophys. Res., 100, 7263–7273, 1995.

Kleffmann, J. and Wiesen, P.: Heterogeneous conversion of NO_2 and NO on HNO_3 treated soot surfaces: atmospheric implications, Atmos. Chem. Phys., 5, 77–83, doi:10.5194/acp-5-77-2005, 2005.

Kleffmann, J., Kurtenbach, R., Lorzer, J., Wiesen, P., Kalthoff, N., Vogel, B., and Vogel, H.: Measured and simulated vertical profiles of nitrous acid – Part I: Field measurements, Atmos. Environ., 37, 2949–2955, 2003.

Kleffmann, J., Gavriloaiei, T., Hofzumahaus, A., Holland, F., Koppmann, R., Rupp, L., Schlosser, E., Siese, M., and Wahner, A.: Daytime formation of nitrous acid: A major source of OH radicals in a forest, Geophys. Res. Lett., 32, L05818, doi:10.1029/2005GL022524, 2005.

Lammel, G. and Cape, J. N.: Nitrous acid and nitrite in the atmosphere, Chem. Soc. Rev., 25, 361–369, 1996.

Title Page

Abstract | Introduction

Conclusions | References

Tables | Figures

|◄ | ►|

◄ | ►

Back | Close

Full Screen / Esc

Printer-friendly Version

Interactive Discussion

Ndour, M., D'Anna, B., George, C., Ka, O., Balkanski, Y., Kleffmann, J., Stemmler, K., and Ammann, M.: Photoenhanced uptake of NO_2 on mineral dust: Laboratory experiments and model simulations, Geophys. Res. Lett., 35, L05812, doi:10.1029/2007GL032006, 2008.

Oncley, S. P., Delany, A. C., Horst, T. W., and Tans, P. P.: Verification of flux measurement using relaxed eddy accumulation, Atmos. Environ., 27, 2417–2426, 1993.

Pattey, E., Desjardins, R. L., and Rochette, P.: Accuracy of the relaxed eddy-accumulation technique, evaluated using CO_2 flux measurements, Bound-Lay. Meteorol., 66, 341–355, 1993.

Ren, X., Brune, W. H., Oliger, A., Metcalf, A. R., Simpas, J. B., Shirley, T., Schwab, J. J., Bai, C., Roychowdhury, U., Li, Y., Cai, C., Demerjian, K. L., He, Y., Zhou, X., Gao, H., and Hou, J.: OH, HO_2, and OH reactivity during the PMTACS-NY Whiteface Mountain 2002 campaign: observations and model comparison, J. Geophys. Res., 111, D10S03, doi:10.1029/2005JD006126, 2006.

Ren, X., Gao, H., Zhou, X., Crounse, J. D., Wennberg, P. O., Browne, E. C., LaFranchi, B. W., Cohen, R. C., McKay, M., Goldstein, A. H., and Mao, J.: Measurement of atmospheric nitrous acid at Bodgett Forest during BEARPEX2007, Atmos. Chem. Phys., 10, 6283–6294, doi:10.5194/acp-10-6283-2010, 2010.

Ren, X., Sanders, J. E., Rajendran, A., Weber, R. J., Goldstein, A. H., Pusede, S. E., Browne, E. C., Min, K.-E., and Cohen, R. C.: A relaxed eddy accumulation system for measuring vertical fluxes of nitrous acid, Atmos. Meas. Tech., 4, 2093–2103, doi:10.5194/amt-4-2093-2011, 2011.

Ridley, B. A. and Grahek, F. E.: A small, low flow, high-sensitivity reaction vessel for NO chemi-luminescence detectors, J. Atmos. Ocean. Tech., 7, 307–311, 1990.

Stemmler, K., Ammann, M., Donders, C., Kleffmann, J., and George, C.: Photosensitized reduction of nitrogen dioxide on humic acid as a source of nitrous acid, Nature, 440, 195–198, 2006.

Stemmler, K., Ndour, M., Elshorbany, Y., Kleffmann, J., D'Anna, B., George, C., Bohn, B., and Ammann, M.: Light induced conversion of nitrogen dioxide into nitrous acid on submicron humic acid aerosol, Atmos. Chem. Phys., 7, 4237–4248, doi:10.5194/acp-7-4237-2007, 2007.

Stutz, J., Alicke, B., and Neftel, A.: Nitrous acid formation in the urban atmosphere: gradient measurements of NO_2 and HONO over grass in Milan, Italy, J. Geophys. Res., 107, 8192, doi:10.1029/2001JD000390, 2002.

Measurements of ambient HONO concentrations

N. Zhang et al.

Title Page

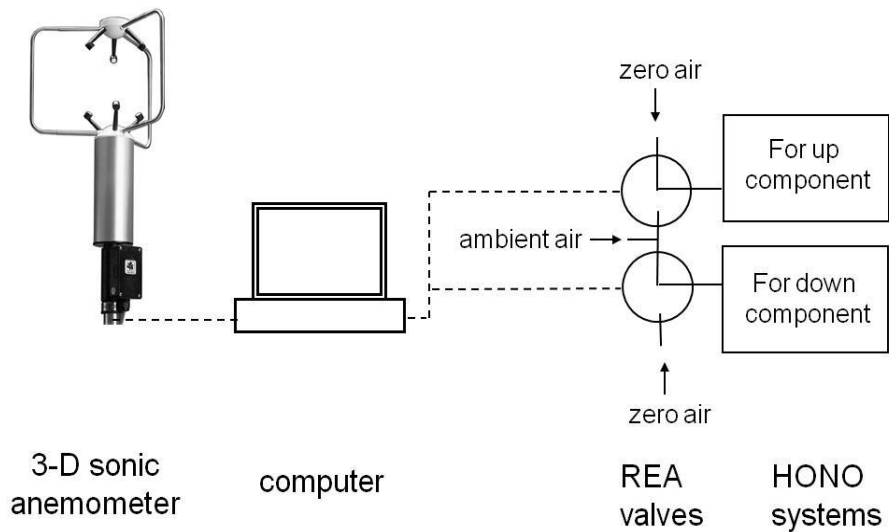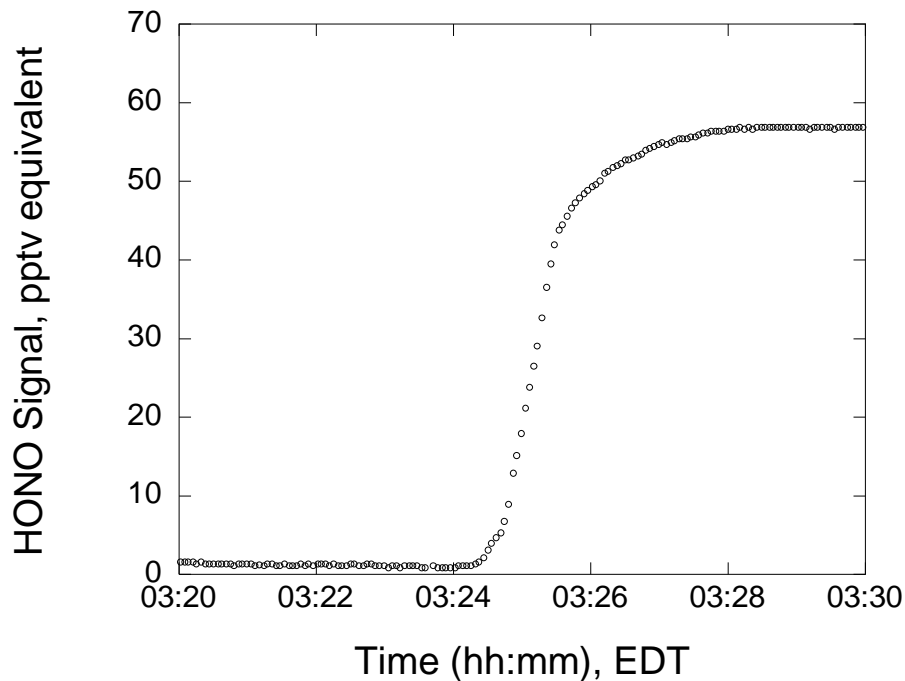| Abstract | Introduction |
| Conclusions | References |
| Tables | Figures |

|◄ | ►|

◄ | ►

Back | Close

Full Screen / Esc

Printer-friendly Version

Interactive Discussion

USEPA publication 625/R-96/010a, Compendium of Methods for the Determination of Inorganic Compounds in Ambient Air: 10-4.2 Determination of Reactive Acidic and Basic Gases and Strong Acidity of Fine Particles, available at: http://www.epa.gov/ttnamti1/, 1999.

Veitel, H., Kromer, B., Mossner, M., and Platt, U.: New techniques for measurements of atmospheric vertical trace gas profiles using DOAS, Environ. Sci. Pollut. R., 4, 17–26, 2002.

Villena, G., Kleffmann, J., Kurtenbach, R., Wiesen, P., Lissi, E., Rubio, M. A., Croxatto, G., and Rappengluck, B.: Vertical gradients of HONO, NO$_x$ and O$_3$ in Santiago de Chile, Atmos. Environ., 45, 3867–3873, 2011.

Vogel, B., Vogel, H., Kleffmann, J., and Kurtenbach, R.: Measured and simulated vertical profiles of nitrous acid – Part II. Model simulations and indications for a photolytic source, Atmos. Environ., 37, 2957–2966, 2003.

Westberg, H., Lamb, B., Hafer, R., Hills, A., Shepson, P., and Vogel, C.: Measurement of isoprene fluxes at the PROPHET site, J. Geophys. Res., 106, 24347–24358, doi:10.1029/2000JD900735, 2001.

Zhang, N., Zhou, X. L., Shepson, P. B., Gao, H. L., Alaghmand, M., and Stirm, B.: Aircraft measurement of HONO vertical profiles over a forested region, Geophys. Res. Lett., 36, L15820, doi:10.1029/2009GL038999, 2009.

Zhou, X. L., Beine, H. J., Honrath, R. E., Fuentes, J. D., Simpson, W., Shepson, P. B., and Bottenheim, J. W.: Snowpack photochemical production of HONO: a major source of OH in the Arctic boundary layer in springtime, Geophys. Res. Lett., 28, 4087–4090, doi:10.1029/2001GL013531, 2001.

Zhou, X., Civerolo, K., Dai, H., Huang, G., Schwab, J., and Demerjian, K.: Summertime nitrous acid chemistry in the atmospheric boundary layer at a rural site in New York State, J. Geophys. Res., 107, 4590, doi:10.1029/2001JD001539, 2002a.

Zhou, X., He, Y., Huang, G., Thornberry, T. D., Carroll, M. A., and Bertman, S. B.: Photochemical production of nitrous acid on glass sample manifold surface, Geophys. Res. Lett., 29, 1681, doi:10.1029/2002GL015080, 2002b.

Zhou, X., Gao, H., He, Y., Huang, G., Bertman, S. B., Civerolo, K., and Schwab, J.: Nitric acid photolysis on surfaces in low-NO$_x$ environments: significant atmospheric implications, Geophys. Res. Lett., 30, 2217, doi:10.1029/2003GL018620, 2003.

Zhou, X., Huang, G., Civerolo, K., Roychowdhury, U., and Demerjian, K. L.: Summertime observations of HONO, HCHO, and O$_3$ at the summit of Whiteface Mountain, New York, J. Geophys. Res., 112, D08311, doi:10.1029/2006JD007256, 2007.

Title Page

Abstract | Introduction

Conclusions | References

Tables | Figures

|◄ | ►|

◄ | ►

Back | Close

Full Screen / Esc

Printer-friendly Version

Interactive Discussion

Zhou, X., Zhang, N., Michaela, T., Tang, D., Hou, J., Bertman, S. B., Alaghmand, M., Shepson, P. B., Carroll, M. A., Griffith, S., Dusanter, S., and Stevens, P. S.: Nitric acid photolysis on forest canopy surface as a tropospheric nitrous acid source, Nature Geosci., 4, 440–443, doi:10.1038/NGEO1164, 2011.

Measurements of ambient HONO concentrations

N. Zhang et al.

Full Screen / Esc

Printer-friendly Version

Interactive Discussion

Table 1. Sampling status in the three HONO measurement systems in a 30-min cycle.

System	"Measurement" (20 min)	"Zero" (10 min)
Updraft	ambient air when $w > w_{\mathrm{T}}$, otherwise zero air	zero air
Downdraft	ambient air when $w < -w_{\mathrm{T}}$, otherwise zero air	zero air
Ambient	ambient air	zero air
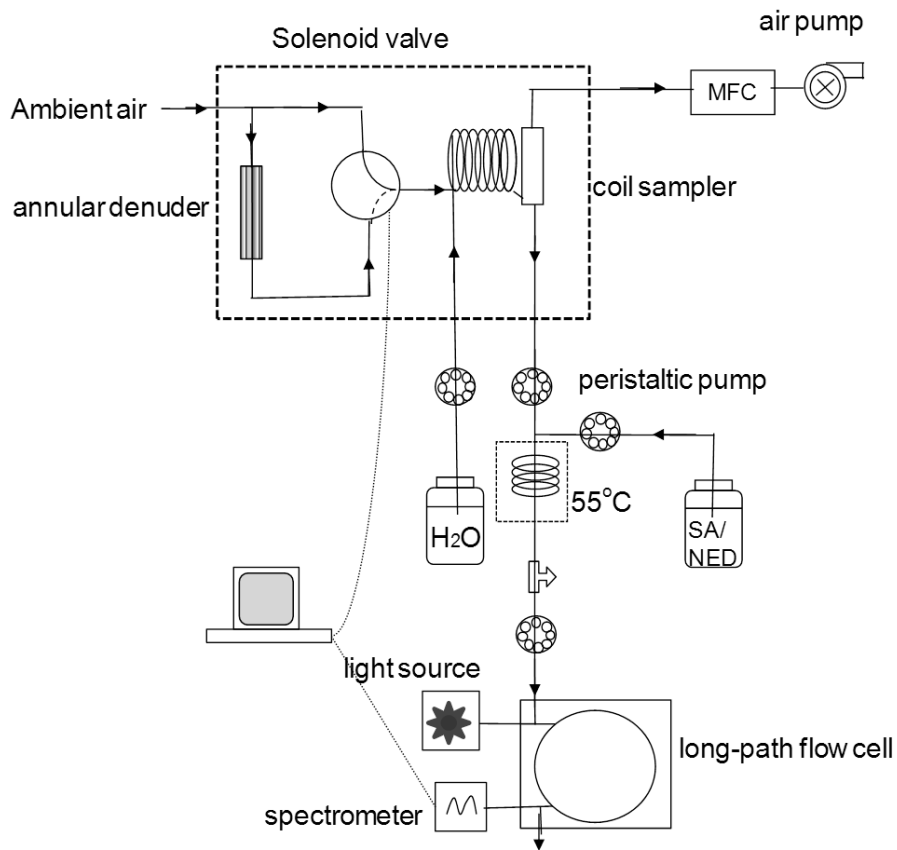
Fig. 1. A schematic diagram of a HONO measurement system.

Fig. 2. A schematic diagram of a REA HONO flux measurement setup, consisting of a 3-D sonic anemometer and two HONO measurement systems.

Fig. 3. An excerpt of 10-min HONO raw data during the transition from the "zero-HONO" base-line to ambient HONO measurement, 25 July 2008. The time in the x-axis is Eastern Daytime-saving Time (EDT, GMT – 04:00).
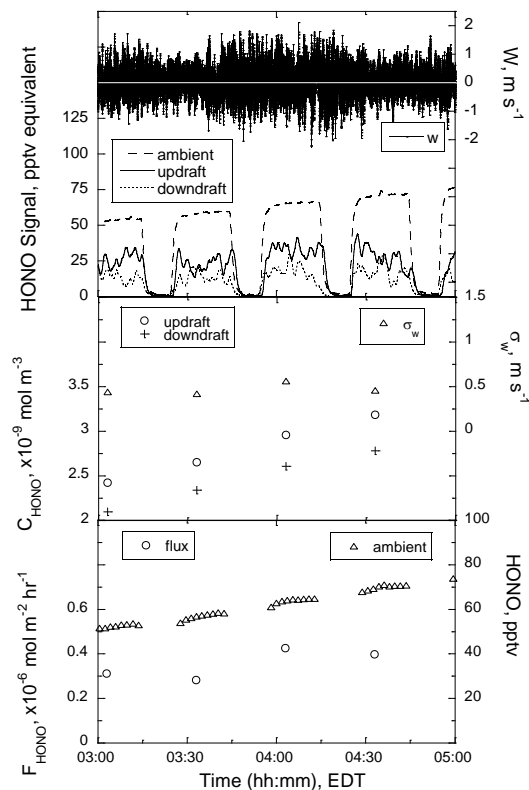
Fig. 4. Examples of raw and processed data collected during a 2-h period on 25 July 2008. Upper panel: raw data of vertical wind speed (10 Hz) and HONO signals (0.3 Hz) from ambient, updraft and downdraft HONO systems. Middle panel: 20-min averages of HONO concentrations in updraft and downdraft air masses, and the standard deviation of vertical wind speed. Lower panel: derived ambient HONO concentrations and flux values.
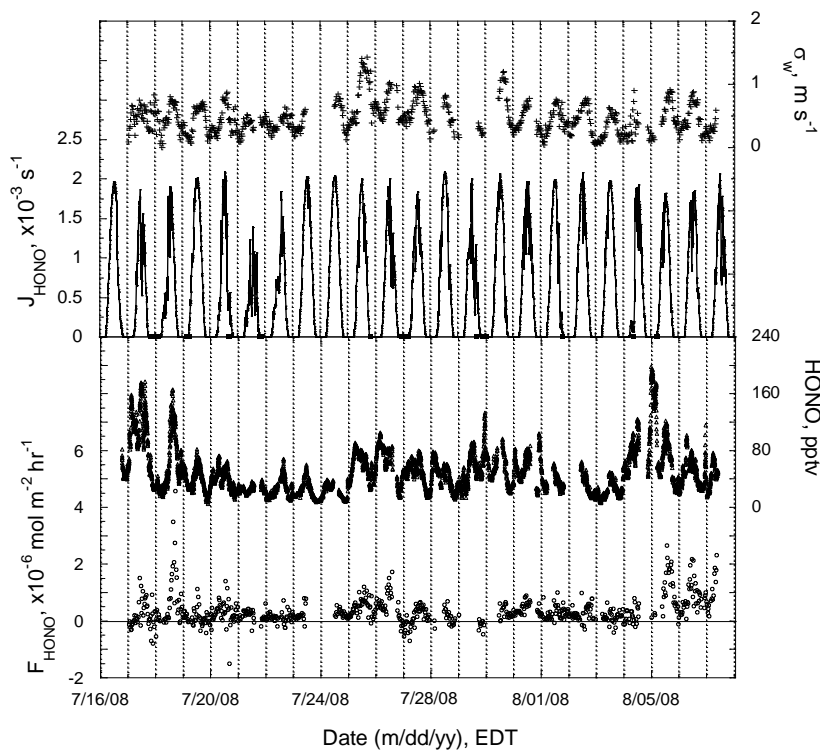
Fig. 5. Time-series of HONO flux (open circles, lower panel, left axis), ambient HONO concentration (open triangles, lower panel, right axis), J_{HONO} (line, upper panel, left axis), and σ_w (cross, upper panel, right axis). The thick horizontal lines at the bottom of the upper panel indicate the periods of rain, mist/fog, or dew events.
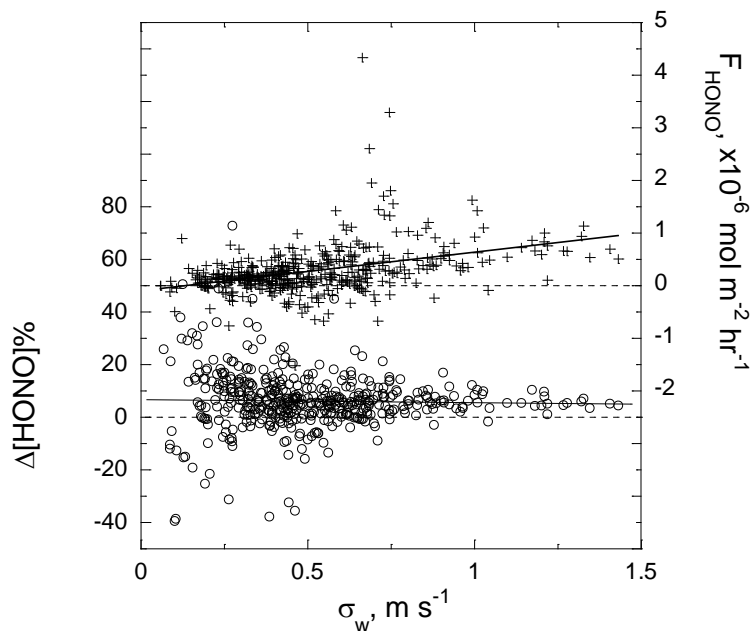
Fig. 6. The percent difference between HONO concentrations (open circles, left axis) in the updraft and downdraft air masses and HONO flux (crosses, right axis) as functions of standard deviation of vertical wind speed.

ACPD

12, 7273–7304, 2012

Measurements of ambient HONO concentrations

N. Zhang et al.

Title Page

Abstract | Introduction

Conclusions | References

Tables | Figures

◄◄ | ►►

◄ | ►

Back | Close

Full Screen / Esc

Printer-friendly Version

Interactive Discussion
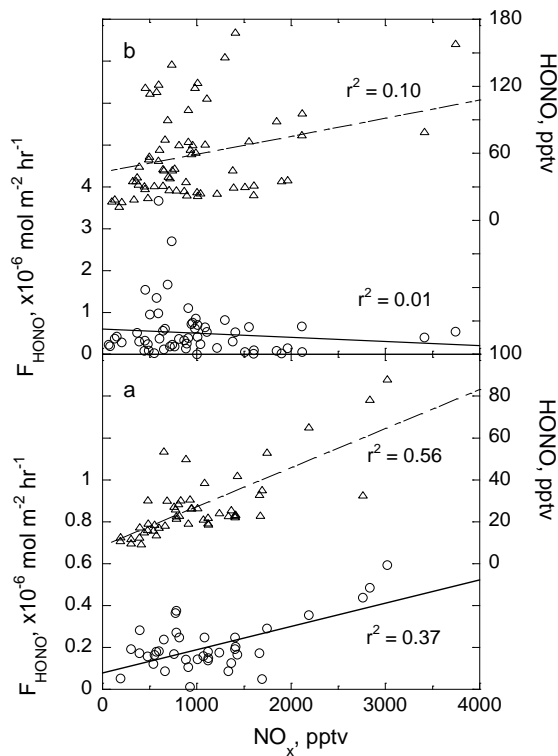
Fig. 7. Correlations between the HONO flux (left axis, open circles) and ambient NO_x concentrations, and between ambient HONO (right axis, open triangles) and NO_x concentrations during the night (22:00–06:00 EDT, **a**) and during the day (08:00–18:00 EDT, **b**). The data are hourly averages, excluding the rain, fog and dew events. The lines are the least-square fits for the data.
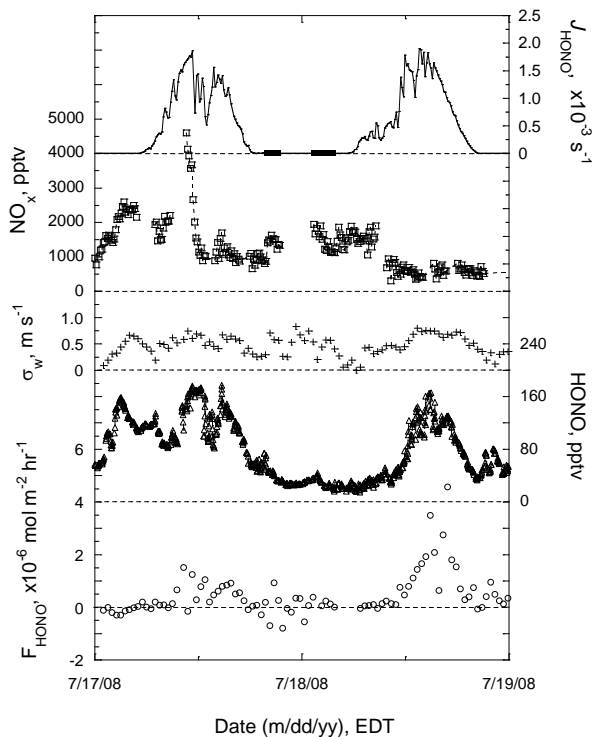
Fig. 8. Two days of time-series of HONO flux (open circles, lower panel, left axis), ambient HONO concentration (open triangles, lower panel, right axis), σ_w (crosses) and NO_x (open squares, upper panel, left axis), and J_{HONO} (line, upper panel, right axis). The two thick horizontal lines at $J_{HONO} = 0$ in the upper panel indicate two periods of light rain.